Nuclear Engineering and Technology 52 (2020) 2151–2161

Contents lists available at ScienceDirect

Nuclear Engineering and Technology

journal homepage: www.elsevier.com/locate/net

Review Article

# Advances in gamma radiation detection systems for emergency radiation monitoring

K.A. Pradeep Kumar [a], G.A. Shanmugha Sundaram [a], B.K. Sharma [b], S. Venkatesh [c], R. Thiruvengadathan [a, *]

[a] SIERS Research Laboratory, Department of Electronics and Communication Engineering, Amrita School of Engineering, Coimbatore, Amrita Vishwa Vidyapeetham, India
[b] Department of Sciences, Amrita School of Engineering, Coimbatore, Amrita Vishwa Vidyapeetham, India
[c] Aparajitha Group, Madurai, India

ARTICLE INFO

*Article history:*
Received 28 May 2019
Received in revised form
8 March 2020
Accepted 11 March 2020
Available online 15 March 2020

*Keywords:*
Gamma radiation detection
Radiation monitoring
Nuclear power plant disaster
Detector active material
Detection platform
Air-borne monitoring
Emergency radiation monitoring

ABSTRACT

The study presents a review of research advancements in the field of gamma radiation detection systems for emergency radiation monitoring, particularly two major sub-systems namely (i) the radiation detector and (ii) the detection platform – air-borne and ground-based. The dynamics and functional characteristics of modern radiation detector active materials are summarized and discussed. The capabilities of both ground-based and aerial vehicle platforms employed in gamma radiation monitoring are deliberated in depth.



## 1. Introduction

Exposure to nuclear radiations is extremely harmful to human and animal life. Three main types of nuclear radiations are alpha, beta, and gamma. Gamma radiation is dangerous to human life causing cellular destruction and subsequently leading to DNA damage, cancer, and radiation sickness if exposed in excess [1]. Gamma radiation detector forms the heart of a radiation monitoring system and hence, deployment of such detectors in the vicinity of nuclear power plants is vital. There has been a steady migration from conventional fossil fuel based energy to the realization of sustainable and economically viable energy. Nuclear reactors have sprung up across the globe to meet the ever-increasing energy demands. As per 2020 statistics, thirty countries are operating 442 nuclear reactors, and 52 new nuclear plants are in the process of being commissioned in 15 countries [2]. It is reported that there has been one major nuclear accident every eight years on an average [2]. Till date, the total number of nuclear accidents is about 100 [3]. Therefore there is a greater need to swiftly evacuate human beings in the vicinity of nuclear reactors and protect them from radiation exposure during such accidents. This has propelled the scientific community to implement improved methods of radiation detection.

On the basis of reported literature, we note that the field of radiation monitoring can be classified into two sub-categories *viz.* (i) Radioactive Pollution Control [4] and (ii) emergency radiation monitoring (ERM). The extent of environmental pollution caused as a result of the regular operation of a nuclear power plant requires continuous monitoring and is henceforth referred as radioactive pollution control. On the other hand, the assessment of radiation contamination resulting from a nuclear accident comes under ERM.

Radioactive pollution control is more mature than ERM technology as measures for controlling nuclear pollution are in place since 1950 [4]. On the other hand, the Three Mile Island accident in 1979 and the Chernobyl disaster in 1986 underscored the importance of ERM procedures [4]. Even the last major nuclear accident in 2011 at Fukushima Power Plant saw an *adhoc* emergency

* Corresponding author.
*E-mail address:* t_rajagopalan@cb.amrita.edu (R. Thiruvengadathan).

https://doi.org/10.1016/j.net.2020.03.014

response strategy which led to confusion and improper emergency evacuation procedures [5]. Furthermore, ERM procedures can be categorized into two classes, *viz.*, ground-based and air-borne monitoring. Though air-borne monitoring was performed immediately after the Fukushima disaster, it took eleven days to process and provide the initial results [6]. Due to the threat of excessive radiation hazard, ground-based monitoring was performed only four days after the catastrophe [5]. Post the Fukushima disaster, there have been significant research advancements made towards establishing mechanisms for ERM. The scope of this article will be confined to reporting ERM aspects of radiation monitoring.

ERM can be conveniently classified into two major divisions *viz.*, the front-end and the back-end systems. The front-end ERM system encompasses components required for gamma radiation measurement and the digitization of the signal corresponding to the measured radiation. The back-end ERM system deals with subsequent analysis as illustrated in Fig. 1.

In the past decade, substantial improvements in detection sensitivity and response time of detector active material have been accomplished. Besides, the major nuclear accident at Fukushima Power Plant has spurred a series of research activities specifically in the deployment of new detection platforms such as mobile robots and unmanned aerial vehicles (UAV). To the best of our knowledge, a comprehensive review article of ground based and aerial monitoring platforms with regard to ERM systems has not been published in the literature. In this paper, we review the research advances reported during the last decade in the public domain by research institutions in the ERM front-end system components – the radiation detector (specifically their performance) and the detection platform. Additionally, technological gaps and the directions for future research are also highlighted.

## 2. Emergency radiation monitoring: Recent research advances

### 2.1. Characteristics of radiation detector

The gamma radiation detector as applied to ERM can be broadly categorized into three classes based on their principle of working. These three classes are the gas-filled detector, the scintillation detector, and the solid-state detector [7,8]. The critical characteristics that serve as a measure of the effectiveness of a radiation detector are: (i) energy resolution, (ii) counting efficiency and (iii) inherent dead time [7]. These characteristics for the three classes of detectors are summarized in Table 1.

#### 2.1.1. Energy resolution

Energy resolution is defined as the ratio of full width half maximum (FWHM) to the corresponding peak energy [8]. Smaller the magnitude of energy resolution better is the energy peak well-resolved [8]. More often energy resolution is measured at 662 keV, which corresponds to Cs-137 gamma source [8].

The number of charge carriers ($N_C$) generated per gamma ray interaction with the active material is a crucial factor that determines the energy resolution of a radiation detector [9]. Energy resolution is inversely related to the square root of $N_C$ [8]. Hence, higher energy resolution is obtained by using an active material that can produce a larger $N_C$ per interaction. This in turn implies that a material with a lower cross section to gamma ray interaction, such as a material of low atomic weight, is seldom efficient in measuring energy. Thus a conventional gas ionization chamber, which uses a relatively lower atomic weight material as an active material, is seldom employed for measuring energy [7]. This has led to the development of the high pressure xenon gas (HPXe) detector, a gas ionization chamber, suitable for measuring energy [10]. A HPXe detector with an excellent energy resolution of 1.7% (Table 1), has been developed by using certain design improvements on a conventional ionization chamber which include the use of low attenuation, thin walled detector [10]. From Table 1 it is evident that the gas-filled detectors have better energy resolution than scintillation detectors [10].

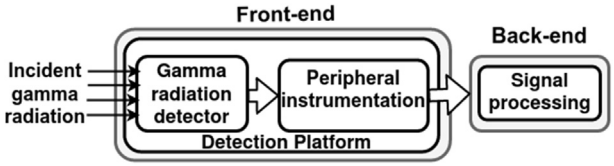


**Fig. 1.** ERM system comprising front-end and back-end components.

The scintillation detector, unlike gas filled and solid-state detectors, requires two stages for converting ionizing radiations to create charge carriers [7]. This results in deterioration of their energy resolution [10]. As seen from Table 1, the energy resolution of modern day scintillation detectors range from 2% to about 4% [11]. Despite their relatively weak resolution, scintillation detector active material can be produced in larger volume than solid state detector. Thus, they are suited for deployment in situations where nominal resolution is sufficient but higher counting efficiency is preferred [10]. Furthermore, compared to a gas-filled detector, a scintillation detector offers a selection from a wide choice of active materials [10].

The energy resolution of solid-state detectors is reported to range from 0.2% to about 2% (Table 1). The energy required to create a pair of charge carrier (electron and hole for solid-state detector) is the smallest for a solid-state detector. Hence, for a given amount of incident ionizing radiation energy $N_C$ is the largest for solid-state detectors [12]. Consequently energy resolution of solid state detectors is superior to gas and scintillation [12]. Among solid-state detectors, High purity germanium (HPGe) is reported to have an excellent resolution of about 0.2% at 662 keV [12]. But, HPGe cannot be operated at room temperature due to its low bandgap [13]. It should be cryogenically cooled using heavy ancillary equipment. This helps to decrease the large leakage current resulting from thermally generated charge carriers [14]. Cadmium zinc telluride (CZT), Cadmium manganese telluride (CMT), Cadmium telluride(CdTe) and Thallium bromide (TlBr) are solid-state detectors operational at room temperature, which dispenses with the need of cooling requirement and is preferred for use in platforms with low payload capacity, such as a battery operated UAV [15]. However, defects in CZT and CMT active material result in charge trapping and consequently degrade their energy resolution [16,17]. James B Ralph and his team at Brookhaven National Laboratory, USA (BNL) have devised techniques that can determine the position of these traps within a CZT crystal and subsequently use appropriate charge correction algorithms to improve energy resolution of CZT based crystals to better than 0.8% at 662 keV [16,17].

An excellent energy resolution of 0.42% using CdTe fabricated as a Shottky diode: Ni/CdTe/Ni has been reported [18]. This is achieved by preventing incomplete charge collection. Incomplete charge collection, in turn, is achieved by operating the diode at a higher bias of 1200 V combined with a CdTe of low thickness of about 1 mm [19].

#### 2.1.2. Counting efficiency

Two types of counting efficiencies, *viz.* absolute and intrinsic efficiency, are generally defined for the three classes of detectors. Absolute efficiency is the ratio of the number of interactions registered by the detector to the number of photons emitted by the

**Table 1**
Recent developments of functional characteristics of the three classes of detector.

| Detector Class | Detector Subclass/Active Material | Energy Resolution at 662 keV | Counting Efficiency at 662 keV | | | | Inherent detector dead-time |
|---|---|---|---|---|---|---|---|
| | | | Absolute | | | Intrinsic | |
| | | | Active material volume ($cm^3$) | Source-detector distance (cm) | % | % | |
| Gas-filled detector | Gas Ionization/HPXe | 1.7% [10] | 200 | 25 | 0.0047 [21] | Not Reported | 650 μs [35] |
| | | | 6255 | 25 | 0.0937 [22] | | |
| | Proportional Counter/GEM (Gas Electron Multiplier) | Not reported | Not reported | | | 0.81 at 59.5 keV [46]<br>0.75 at 122 keV [46] | 10 μs [46] |
| | Geiger Muller Counter/Micro-discharge based radiation detector | Not applicable | Not reported | | | 4 [24] | 1–10 μs [32] |
| Scintillation detector | PVT (Polyvinyltoluene) | 25% at 1 MeV [47] | 58473 | 25 | 0.0223 [22] | 39 [25] | 41.6 ns [48] |
| | $LaCl_3$:Ce (Lanthanum chloride) | 3.8% [26] | 103 | 25 | 0.0767 [22] | 23.3 [26] | 64 ns [49] |
| | $CeBr_3$:Sr (Cerium bromide) | 3% [36] | Not reported | | | Not reported | 57 ns [49] |
| | $K_2BaI_4$:Eu (Potassium barium iodide) | 2.9% [50] | Not reported | | | Not reported | 760 ns [50] |
| | $LaBr_3$:Ce (Lanthanum bromide) | 2.66% [27] | 12.87 | ~0 | 5.3 [23] | 33.8 [27] | 56 ns [49] |
| | | | 12.87 | 5 | 1.2 [23] | | |
| | | | 12.87 | 10 | 0.5 [23] | | |
| | | | 12.87 | 15 | 0.00027 [23] | | |
| | | | 12.87 | 25 | 0.0001 [23] | | |
| | $KSr_2I_5$:Eu (Potassium strontium iodide) | 2.4% [51] | Not reported | | | Not reported | 1030 ns [51] |
| | $KBa_2I_5$:Eu (Potassium barium iodide) | 2.4% [50] | Not reported | | | Not reported | 950 ns [50] |
| | $CsBa_2I_5$:Eu (Cesium barium iodide) | 2.3% [37] | Not reported | | | Not reported | 1040 ns [52] |
| | $LaBr_3$:Ce,Sr | 2% [53] | Not reported | | | Not reported | 58 ns [53] |
| | $GdBr_3$:Ce (Gadolinium bromide) | >10% [38] | 12 | ~0 | 2.7 [38] | Not reported | 95 ns [38] |
| Solid-state semiconductor detector | CMT | 2.1% [54] | Not reported | | | Not reported | ~100 ns [8] |
| | TlBr | 1.6% [55] | Not reported | | | Not reported | ~100 ns [8] |
| | CZT | 0.6–0.81% [16,17,56] | 1 | 25 | 0.00098 [22] | ~7 [28,29] | ~100 ns [8] |
| | CdTe | 0.42% [18] | 23.11 | ~0 | 1.2 [57] | Not reported | ~100 ns [8] |
| | HPGe | 0.2% [12] | 347.5 | 25 | 0.2 [22] | 2 [58] | ~100 ns [8] |

source [8]. It is dependent on the distance between the source and the detector, as well as the volume and the density of the active material [20]. The absolute efficiency for HPXe (Gas filled detector) with an active material volume of 200 $cm^3$ is reported to be 0.0047% for a source-detector distance of 25 cm [21]. About twenty times rise in efficiency to 0.0937% is noticed when the active material volume is increased by nearly thirty times to 6255 $cm^3$ [22]. The efficiency reported for scintillation detectors ranges from 0.0001% to 0.0767% [22,23]. It is evident from Table 1 that for an equivalent active material volume, scintillation detector is reported to have a higher absolute efficiency than the gas-filled detector. Table 1 also presents the dependence of absolute efficiency with variation in the distance between source and detector for a scintillation detector. The efficiency is 5% with the source touching the front-face of the detector and drops to 0.5% with the distance increased to 10 cm [23]. For a distance beyond 15 cm, the efficiency drops drastically and approaches zero percent [23]. For the solid-state detectors, the reported efficiency ranges from 0.00098 to 0.2%. Absolute efficiency of scintillation and solid-state detectors with comparable active material volume are reported to be similar [22].

Intrinsic efficiency is the ratio of the number of interactions registered by the detector to the number of photons incident on the detector [8]. Unlike absolute efficiency, intrinsic efficiency is a relative measure and is independent of the distance between the source and the detector [20]. Comparison of intrinsic efficiency of active materials is presented in Table 1. Typical intrinsic efficiency of GM counters is 0.5–1.5% [24]. A variant of GM counter utilizes a micro machined stack structure to increase intrinsic efficiency to as high as 4% [24]. The intrinsic efficiency of modern scintillation detectors ranges from about 23 to 39% [25–27]. Intrinsic efficiency of room temperature solid-state active material is severely limited by the ability to utilize a large volume (>1 $cm^3$) crystal to achieve simultaneously good energy resolution and counting efficiency [28,29]. Large volume crystals tend to have deteriorated energy resolution due to severe hole trapping [28,29]. Kai Vetter et al. and Luke et al. have employed a coplanar-grid technique to create novel detector designs, which permits the employment of large volume crystal and consequently achieve intrinsic efficiency as high as 7% without compromising on energy resolution [28,29].

### 2.1.3. Inherent detector dead time

Besides energy resolution and counting efficiency, the other parameter of interest is inherent detector dead time. Dead time is the duration during which the detector system is busy processing a gamma radiation interaction and is unresponsive to newer gamma interactions [30]. The dead time for a detector system can be conveniently considered to be an aggregate of three components – namely inherent detector dead time, pulse processing dead time and multichannel analyzer dead time. While pulse processing dead times and multichannel analyzer dead times are dependent on electronics used, the inherent detector dead time is dependent on the active material. We focus only on the inherent detector dead time for the sake of comparison of this parameter for the three classes of detector. Smaller the value of inherent detector dead time, faster is the detector response [31]. Inherent detector dead

time is the time required for the generation of a pulse within the detector active material [31]. Gas filled detectors have the largest inherent dead time in the order of 10 μs to hundred microseconds (Table 1). It is interesting to note from Table 1 , that though the conventional GM detectors had dead times in the order of 100 μs, recent GM detectors have been reported to have much lower inherent dead time in the order of 1 μs [32]. The inherent dead time of scintillation detector is the sum of primary decay constant and average electron transit time of PMT (time taken for electrons to travel from photocathode to an anode) [33,34]. The typical electron transit time of a modern PMT is 20–40 ns [33,34]. Hence, the inherent detector dead time of scintillation detectors in Table 1 includes 40 ns in addition to the primary decay constant of the scintillation detector crystal. Inherent detector dead time of scintillator detector is the lowest among all classes of detectors (Table 1) [31]. Typical inherent detector dead time of solid-state detector, irrespective of the active material deployed, is approximately 100 ns [8]. Nearly all of the active material need a typical operating bias voltage from 500 V to 1500 V [22,24,26,27,35–40]. However, scintillation active materials coupled to a silicon photon multiplier (SiPM) instead of a photomultiplier tube(PMT) require only a lower bias voltage ranging from 25V to 75 V [41,42].

Active research is in progress to obtain good energy resolution high-Z sensitized plastic scintillators (which has a distinct merit of being affordable and available in large volumes) by blending it with fluoride and oxide nano-particles [43]. Further, halide perovskite based nano-materials are being investigated for use as gamma radiation detection active materials [44,45]. The functional characteristics of other active materials are given in Table 1 [46–58]. Specifically, $CsPbBr_3$, a halide perovskite, has been demonstrated to have an excellent energy resolution of 3.8% [59].

An ERM system must be able to monitor a substantial amount of radiation. However, it is equally essential for the ERM system to detect small but harmful radiation limits. To appreciate the role of a radiation detector active material in measuring a subtle amount of radiation, we consider a crucial detector parameter viz. detection sensitivity. The detection sensitivity, $S_D$, of a detector is defined as the smallest change in the radiation intensity that it can reliably measure [60] and is given by Eq. (1) [61].

$$S_D = \frac{k}{s\varepsilon(E)}\sqrt{\frac{f_{bkg}(E)R(E)}{t_{int}}} \quad (1)$$

In Eq. (1), $R(E)$ is the energy resolution, $\varepsilon(E)$ is the counting efficiency, $t_{int}$ is the integration time, $s$ is the count-rate sensitivity of the detector, $f_{bkg}(E)$ is the background radiation intensity and $k$ is the proportionality constant. We analyze three different active material, one from each detector class, namely CZT, LaBr3:Ce, and Micro-discharge based radiation detector. We substitute the efficiency and resolution values listed for these active materials in Table 1 into Eq. (1). We sketch the detection sensitivities of the detectors employing these active materials as a function of source-detector distance (Fig. 2). It must be emphasized here that lower the detection sensitivity, better is the detector performance. Scintillation detectors offer the best detection sensitivity, followed by solid-state detectors. In particular, LaBr3:Ce offers a detection sensitivity of about three times lower than CZT and fifty times lower than the micro-discharge based detector. The detection sensitivity falls exponentially with source-detector separation, and the intervening material (usually air) decides the rate of increase. However, employing a gas-filled detector offers certain attractive features such as easy fabrication, active material non-degradation due to irradiation, the feasibility of construction of detectors with varying sizes and shapes [7]. Thus, in addition to the three critical detector parameters discussed in this section, other parameters such as cost, weight, commercial availability, ease of fabrication, cooling, and power source requirements also influence the choice of a particular detector for ERM.

Deployment of a particular detector class in an ERM system, in addition to being influenced by energy resolution, efficiency and dead time, is also dependent on the arrangement by which the active material is mounted. The following section deals with the aerial and the ground platforms and the associated merits and demerits in the deployment methods.

### 2.2. Detection platform

Apart from the characteristics of the detector systems discussed above, the vehicle and the mode of its deployment is a critical issue. We, therefore, highlight the practical, yet innovative approaches that have been employed in the aftermath of most recent nuclear accident at Fukushima. Gamma rays' emission during a nuclear accident can be monitored by installing detection system on the ground or from an aerial platform. The three primary tasks reported to be performed by the detection platform are (i) mapping fallout, (ii) localization, and (iii) plume tracking. Mapping fallout describes the spatial distribution of radioactive ground contamination and is done with the help of total radioactivity count rate (radiation intensity) measure [62]. Usually, a detector active material with a high counting efficiency is preferred for mapping fallout [60]. Localization is the process of locating hotspots, which are defined as pockets of relatively higher radioactive surface contamination [63]. Gamma-ray spectrometry is employed to analyze all of the isotopic constituents of the hotspot. Typical radionuclide species examined in the hotspot include $^{137}Cs$, $^{134}Cs$, $^{131}I$, $^{129m}Te$, $^{110m}Ag$, $^{238}Pu$, $^{239+240}Pu$, $^{89}Sr$ and $^{90}Sr$ [64]. Frequently, a detector active material with an excellent energy resolution is employed for localization [60]. Mapping fallout is associated with the creation of ground contamination radiation maps and does not care about the location of a radioactive point source. In contrast, localization uses the contamination map as a guide to discover the point source. Plume tracking is performed to detect the boundary and track the movement of the concentrated radioactive mass released into the atmosphere [62].

#### 2.2.1. Ground-based ERM

Ground-based ERM can be performed either using fixed or mobile detectors. A summary of characteristics of recent ground-based radiation monitoring systems are presented in Table 2 [65–75]. In fixed ground monitoring, ERM is carried by mounting

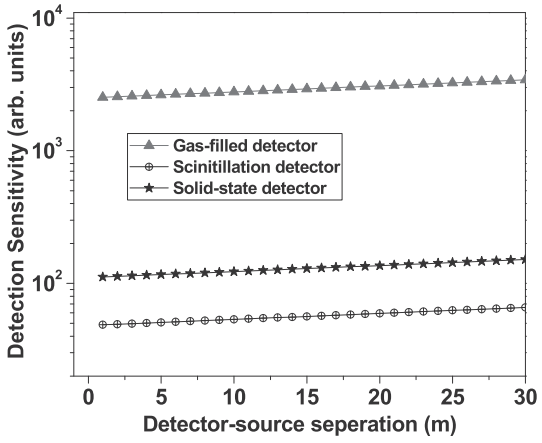


**Fig. 2.** Detection sensitivity of three classes of detectors.

**Table 2**
Recent ground-based radiation monitoring systems.

| Installation Type | Application | Gamma Radiation Detector Class/Active material | Detection Sensitivity (nSv/h) | Integration time(s) | Upper detection Limit (mSv/h) | System/Contributors/Year |
|---|---|---|---|---|---|---|
| Fixed, Man-borne | Mapping fallout | GM Counter | 4.4 | 180 | Not reported | Garcia et al./2018 [65] |
| Man-borne | Localization | Scintillation/NaI(Tl) | 60 | Not reported | Not reported | Kaniu et al./2018 [66] |
| Fixed | Mapping fallout | GM Counter | 50 | 10 | 1000 | Susila et al./2017 [67] |
| Man-borne | Localization | Scintillation/CsI(Tl) | 1000 | 900 | 0.019 | Yasutaka et al./2016 [68] |
| Mobile robot | Mapping fallout | GM Counter | Not reported | Not reported | 10 | Raúl et al./2015 [69] |
| Vehicle-borne (cargo truck) | Localization | Solid-state/HPGe Scintillation/CsI(Tl) | 56 | 5 | 0.1 | Radi-probe/2015 [70] |
| Vehicle-borne (car) | Mapping fallout/Localization | Scintillation/NaI(Tl) Solid-state/HPGe | Not reported | Not reported | Not reported | Syarbaini et al./2015 [71] |
| Vehicle-borne (car) | Mapping fallout | Scintillation/CsI(Tl) | 100 | 3 | 0.019 | Kurama II/2015 [72] |
| Vehicle-borne (car) | Mapping fallout | Scintillation/NaI(Tl) | 100 | 3–10 | 0.019 | Kurama/2013 [73] |
| Vehicle-borne (car) | Mapping fallout/Localization | Proportional Counter, Scintillation/NaI(Tl), Solid-state/HPGe | 100 | 10/180 | 100 | Baeza et al./2013 [74] |
| Man-borne | Mapping fallout | Solid-state/Silicon PIN photo diode | 50 | 1200 | Not reported | Yang et al./2013 [75] |

the detectors on fixed installation. In contrast, in mobile ground monitoring, the detectors are moved on land by a mobile platform. The mobile platform could be a vehicle, a robot or man-borne [75]. The choice of the active material employed in the detector is dictated by its ability to measure and record mapping fall out and source localization with high reliability and precision.

Ground-based ERM is invariably carried out first following a nuclear accident due to its ease of operation [76]. Also, ground-based ERM can be performed even during unfavorable weather conditions [76]. Further, ground-based ERM can be achieved quite easily at positions within a nuclear facility. Such locations may not provide direct line of sight required for operating an air-borne ERM [69].

The characteristics reviewed include detection sensitivity, integration time and upper detection limit. In turn, these parameters are influenced by energy resolution, counting efficiency and dead time of detector discussed in the previous section. For a ground-based radiation monitoring system, detection sensitivity is a function of source-detector distance, integration time (exposure time of the detector) and the volume of radiation detector active material [60,77]. Detection sensitivity of ground-based systems reported in Table 2 ranges from 4.4 nSv/h to 100 nSv/h measured at a source-detector distance of 1 m with integration time varying from 3 to 1200 s. Typical value of integration time for mapping fallout (excluding man-borne systems) is 10 s whereas that for performing gamma-ray spectrometry required for localization is in the order of 100s of seconds [78]. Smaller integration time leads to better spatial resolution, which is defined as the measure of the ground area imaged by the instantaneous detector field of view [79,80]. At the same time, larger integration time leads to better signal to noise ratio of the gamma radiation spectrum of the ground radiation source [79,80]. Thus an optimum value for integration time is a tradeoff between spatial resolution and signal to noise ratio requirements of the gamma radiation spectrum [81]. Upper detection limit is the maximum dose rate the detector can be exposed to before it gets saturated due to a finite detector dead time [60]. The fixed ground based detection system with a GM counter reported by Susila et al. has a very high upper detection limit of 1000 mSv/h [67]. On the other hand, Kurama (Kyoto university radiation mapping system), a mobile ground based scintillation detection system is reported to have a low upper detection limit of 19 μSv/h [72]. A system with a higher upper detection limit has the advantage of being operable more reliably in radioactive environments with very high gamma rate exposure. From Table 2, it is apparent that for ground-based ERM, GM counter and sodium iodide activated with thallium (NaI(Tl)) based scintillation counters are the most prevalent detector deployed for mapping fallout [65,67,69,71,73,74]. HPGe based solid-state detector is usually employed for localization [70,71,74].

In the aftermath of the accident at the Fukushima Nuclear power plant, an innovative approach to employing a smartphone-based radiation monitoring network is being implemented [75]. In this approach, the community is requested to involve and participate as a volunteer. Each volunteer buys a low-cost silicon PIN photodiode, a solid state semiconductor class of detector that is integrated with a smartphone. The phone acts as a radiation detection device and reports the GPS location and radiation intensity recorded by the instrument to a central authority. The authority processes the information flowing in from all the volunteers currently logged in and provides a near-real-time radiation fallout map around the site. The other man-borne systems are reported by Yasutaka et al., Kaniu et al. and Garcia et al. Man-borne units serve the purpose of human re-habitability readiness check in a nuclear disaster-prone region/building or act as a smartphone based radiation detector that can replace a conventional personal dosimeter typically used by radiation exposed personnel [64,65,71].

The vehicle-borne system reported by Baeza et al. in addition to being a conventional car-borne system, also serves as a mobile lab that can assist analysis of radioactivity in soil samples [74]. The mobile lab is an autonomous unit with the whole process of gamma radiation acquisition and storage/display completed within the lab. The car-borne system related by Syarbaini et al. is a similar autonomous system [71].

In contrast to the use of the autonomous mobile detector platforms discussed above, Kurama utilizes a fleet of cars, with the data acquired using LabView© and shared using Dropbox©, a cloud-based data distribution software [73]. The radiation detector is installed within the vehicle, which necessitates incorporating a complicated correction factor, to obtain a true radiation count. Kurama-II is an enhanced version of Kurama [72]. It implements a built-in computer attached to the radiation detector. Radi-probe is a vehicle-borne system complementary in nature to Kurama hosting a gamma spectrometry and deployed on a cargo truck [70].

In general, the hotspots in the reactor core and its surrounding region in a nuclear plant require detection systems with high spatial resolution. Car-borne methods may not be safe in such a scenario for the personnel operating the vehicle. In this context, Raúl M. Vázquez et al. have successfully deployed a mobile land-

**Table 3**
Summary of characteristics of recent aerial-based radiation monitoring systems.

| System | Power Source | Payload Weight (kg) | Gamma Radiation Detector | Primary Application/ Vehicle Type | Maximum Detection Distance Limit (m) | Integration time(s) | Contributors/Year |
|---|---|---|---|---|---|---|---|
| Compton camera based Unmanned Multicopter drone | Battery | 1 | Ce:$Gd_3(Al,Ga)_5O_{12}$ (Ce:GAGG) | Localization/Unmanned Multicopter | 9 | 180 | Yuki Sato et al. (2018) [92] |
| DJI S1000+ Compton camera based Unmanned Octocopter | Battery | 11 | Ce:$Gd_3(Al,Ga)_5O_{12}$ | Localization/Unmanned Octocopter | 20 | 790 | S. Mochizuki et al. (2017) [93] |
| Improved GAGG Compton camera based Unmanned Helicopter | Battery | Not specified | Ce:$Gd_3(Al,Ga)_5O_{12}$ | Mapping fallout/Unmanned Helicopter | 35 | 1 | Y. Shikaze et al. (2016) [94] |
| AirRAM 2000 | Vehicle Fuel | 50 | NaI(Tl), Geiger Mueller | Plume Tracking, Mapping fallout/Manned Helicopter | 50 | 2 | Dadon et al. (2016) [91] |
| RMAX G1 Autonomous Unmanned Helicopter | Vehicle Fuel | 10 | $LaBr_3$:Ce | Localization/Unmanned Helicopter | 100 | 100 | Sanada et al. (2015) [95] |
| Haptic guided UAV | Battery | 4 | CZT | Localization/Unmanned Helicopter | 2 | 4 | Micconi et al. (2015) [90] |
| AARM-X8, multirotor aerial vehicle | Battery | Not specified | CZT | Mapping fallout/Unmanned Helicopter | 15 | 2 | Martin et al. (2015) [96] |
| URSAS/Aeroscout B1-100 | Battery | 9 | NaI(Tl) | Mapping fallout/Unmanned Helicopter | 40 | 1 | Kevin et al. (2014) [89] |
| Hexa XL, Mikrokopter | Battery | Not specified | CZT | Localization/Unmanned hexacopter aerial system | 3 | 800 | MacFarlane et al. (2014) [6] |
| Aeroscout B1-100 Unmanned Systems Laboratory | Vehicle Fuel | 20 | NaI(Tl) | Mapping fallout/Unmanned Helicopter | 60 | 1 | Jerry Towler et al. (2012) [88] |
| CEA-LIST X4 Flyer | Battery | 0.2 | CZT | Localization/ UnmannedHelicopter | 2 | 300 | K. Boudergui et al. (2011) [97] |
| Patria mini-UAV/ MASS, modular airborne sensor system | Not Reported | 0.5 | CsI | Mapping fallout/Unmanned Aircraft | 50 | 1 | Roy Pöllänen et al. (2009) [98] |
| RMAX, Yamaha Co. AUH | Vehicle Fuel | 8.5 | PVT | Mapping fallout/Unmanned Helicopter | 100 | 1 | Shinichi-Okuyama et al. (2008) [99] |

based robot radiation detector system that can be monitored remotely from a distance of one km [69].

Since the spread of radiation can easily extend into several tens of kilometers from the location of the reactor, in the event of a nuclear catastrophe, a ground-based monitoring system may not be practically applicable due to financial constraints and possible safety and security-related issues [62,82]. Specifically, the ground-based radiation detector is practically applicable only on a small region. Another shortcoming of a ground-based detection system could be the non-availability of proper roads in remote locations [83]. For example, thick vegetation, abrupt slopes and water passages around the nuclear plant could be some of the causes for non-availability of roads [83]. An alternative and yet an attractive proposition to ground-based monitoring of radiation is air-borne detection systems, detailed in the next sub-section.

### 2.2.2. Air-borne ERM

Air-borne radiation monitoring provides a larger field of view, which is about 100–1000 times more than ground-based monitoring system [84]. Modern air-borne systems can be used to monitor high levels of radiation through the use of real-time monitoring methods at safe altitudes [63]. Either a helicopter or a fixed winged aircraft is utilized as an air-borne vehicle. Helicopters fly at low altitudes of 15 m and can provide better spatial resolution for fallout mapping than using an airplane [76]. Further, a helicopter has the capability to hover and hence is suitable for performing localization of hotspots [76]. At the same time, the cost of operating a helicopter is higher than fixed winged aircraft, and it has also lower speed and smaller flight endurance (typically 2 h), limiting its efficiency to monitor relatively smaller areas [76,85].

A fixed-wing aircraft has to maintain a minimum safe ground clearance of about 30 m. Surveys performed at an altitude of 30 m are called low-level surveys and results in a spatial resolution of 150 m [76]. Surveys done at an elevation of 150 m and above are called large-scale surveys and results in a spatial resolution greater than 300 m [86]. However, the spatial resolution obtained from fixed-wing aircraft is very poor, therefore only a pseudo average of ground contamination spread throughout an approximate diameter of 300 m or higher is obtained in high-level surveys.

Shinichi Okuyama et al. developed a UAV for plume tracking [87]. This UAV had not been designed for mapping fallout and localization of hotspots. Motivated by the lack of deployment of UAV based radiation monitoring during Fukushima disaster, Unmanned Systems Laboratory at Virginia Tech, developed and tested

UAV based radiation monitoring system that can be used for mapping fallout and localization of hotspots [88]. The UAV developed by Unmanned Systems Laboratory weighs 90 kg including payload and the active detection material used is NaI(Tl). MacFarlane et al. developed an ultra-lightweight, battery powered system with a high spatial resolution of less than 1 m [6]. The UAV is loaded with a light weight, small volume room temperature CZT detector. The UAV is capable of mapping fallout but in offline mode and needs to be operated at very low altitudes typically in the orders of 3 m due to the low sensitivity of the solid-state detector in comparison to large volume scintillation detectors. Extreme care has to be exercised in safeguarding the UAV from possible obstacles due to very little ground clearance of 3 m. The UAV developed by Kevin et al. is capable of autonomously deploying a robot to collect a ground contaminated sample for offline processing and retract the robot back to the vehicle [89]. The system produced by Micconi et al. is competent of being guided by a human operator using visual and force feedback [90]. Force feedback is provided using a haptic interface. Maximum flight altitude is just 2 m but the system is capable of providing spectrum information in less than 4 s. Further, the system can detect gamma radiation corresponding to a dose rate as low as one mSv/year, which is the prescribed safety limit for radiation-exposed personnel. AirRAM 2000 is a manned helicopter system specially developed for radioactive plume tracking and is proficient of performing real-time gamma spectroscopy as well [91]. The UAVs developed by Shikaze et al., Mochizuki et al., and Yuki Sato et al. utilize a Compton camera for radiation monitoring [92–94].

Table 3 summarizes the capabilities of air-borne ERM systems developed during the past decade [92–99]. Specifically, Table 3 lists aerodynamic endurance factors, namely power source and payload weight, which also influence detection capabilities. However, in this review, we will only briefly consider these parameters. It is interesting to observe that the GM counter is the only gas-filled detector listed in Table 3 [95]. GM counter has excellent dose rate detection sensitivity as a consequence of its relatively high count-rate efficiency as can be inferred from Eq. (1). From Table 3, it could be understood that the focus of the development of ERM systems has changed from manned to unmanned vehicle. Most recent advancements are on developing systems capable of performing gamma-ray spectrometry using ultra-lightweight unmanned aerial vehicles [96]. Solid-state detector, CZT is reported to be the preferred detector used in battery operated lightweight UAVs [6,90,96,97]. Newer scintillation detector such as LaBr3:Ce is used in higher payload capacity UAVs [95].

The definite advantage of aerial radiation monitoring is the larger field of view, thereby facilitating the creation of radiation maps much faster than ground-based radiation monitoring. The field of view can be improved with an increase in aircraft altitude but is limited by the detection sensitivity of the system. Fig. 3 presents a comparison of the variation of count-rate sensitivity of the aerial systems with the altitude of the vehicle. Fig. 3 includes only those findings that have incorporated a background count rate correction. The simplest way to perform a background correction is to (i) acquire the background radiation in the absence of the radioactive source, (ii) measure radiation in the presence of radioactive source and (ii) then subtract the background radiation obtained in (i) from the composite signal recorded in (ii) [100]. The second method of background correction relies on gamma spectroscopy. The isotope of interest and background radioactive emitters have different spectral signatures [101]. Therefore, the peaks due to background radioactive emitters can be eliminated, leading to a background-corrected signal [101,102]. The third method of background correction is necessary in situations that demand a short acquisition time, typically in the order of a few seconds. The gamma spectrum collected for such a short span does not present noticeable spectral signatures needed for background subtraction [101]. Complex background correction algorithms are needed in such scenarios [101,103,104]. The count-rate sensitivity presented in Fig. 3 relates to the total radioactive count rate in counts per second (cps) recorded by the radiation detector for a representative dose rate of 1 μSv/h located on the ground. The count-rate sensitivity, *s*, as related in Eq. (1), is inversely related to the detection sensitivity, $S_D$. From Fig. 3, it is evident that the count-rate sensitivity has increased about 50 times in 2015 in comparison to that reported in 2008 for fuel based aerial systems. The battery operated system reported by Shikaze et al. in 2016 has lower count-rate sensitivity than that reported by Okuyama et al. in 2008 [94,99]. Fuel based aerial systems have higher payload capability than battery operated vehicles. This facilitates deploying heavier and hence larger volume active material in a fuel based aerial vehicle leading to better count-rate sensitivity and a higher maximum detection limit between 50 m and 100 m [88,91,95]. Performing a partial differentiation of '*s*' in Eq. (1) with respect to height, we can obtain the slope of *s* and infer that the slope is inversely proportional to the square of detector efficiency. Thus lower detector efficiencies lead to sharper gradients. Hence battery operated vehicles have a lower maximum detection limit ranging from 2 m to 40 m [6,89,90,92–94,96–98].

We conclude this section by analyzing the detection sensitivities of the systems discussed until now. To make an unbiased comparison across these heterogeneous platforms, we will use a normalized form of Eq. (1) by setting $f_{bkg}(E)$, $k$ and $s$ to unity. The resultant expression is given by Eq. (2) and Eq. (3) [105]. By normalizing, we ensure that all the detection systems examined are subjected to the same background and surface radioactivity.

$$S_{DN} = \frac{1}{\varepsilon(E)}\sqrt{\frac{R(E)}{t_{int}}} \tag{2}$$

$$\varepsilon(E) = \frac{A_d}{4\pi d^2} e^{-\mu_{air} d}\left(1 - e^{-\mu_{act} t_{act}}\right) \tag{3}$$

In Eq. (3), $d$ is the source-detector distance, $t_{act}$ is the active material thickness and $A_d$ is the cross-section area of the active material perpendicular to the incident gamma radiation. Further, $\mu_{air}$ and $\mu_{act}$ are the linear attenuation coefficient of air and detector active material to gamma radiation at 662 keV respectively [106] . We use the values listed in Table I and Table 4 to evaluate Eq. (2) and

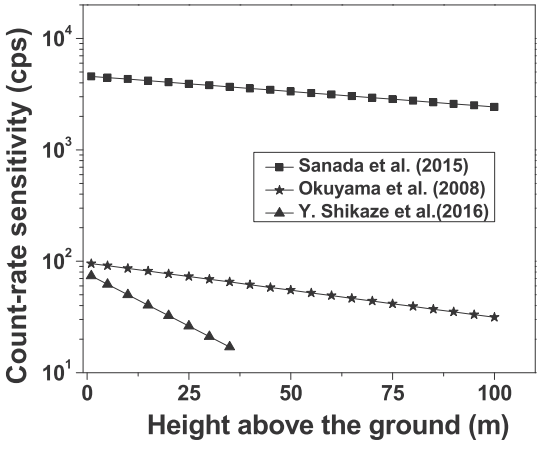


**Fig. 3.** Variation of count-rate sensitivity with altitude of aerial vehicle for 1 μSv/h dose rate.

**Table 4**
Values used for evaluation of relative detection sensitivity.

| Contributors | $d$ (m) | $t_{act}$ (cm) | $A_d$ ($cm^2$) | $\mu_{act}$ ($cm^{-1}$) | $t_{int}$ (s) |
|---|---|---|---|---|---|
| Susila et al. [67] | 1 | 31 | 39.25 | 0.0001 | 10 |
| Kurama II [72] | 1 | 2 | 1.69 | 0.3776 | 3 |
| Karama I [73] | 1 | 2.54 | 6.4 | 0.2782 | 3 |
| Baeza et al. [74] | 1 | 5.08 | 5.06 | 0.2782 | 10 |
| Yang et al. [75] | 1 | 0.09 | 1 | 0.1882 | 1200 |
| Shikaze et al. [94] | 35 | 1.5 | 1 | 0.5566 | 1 |
| AirRAM [91] | 50 | 5.08 | 40.52 | 0.2782 | 2 |
| Micconi et al. [90] | 2 | 0.6 | 4 | 0.4621 | 4 |
| Martin et al. [96] | 15 | 0.6 | 0.4 | 0.4621 | 2 |
| Kevin et al. [89] | 40 | 7.62 | 45.58 | 0.2782 | 1 |
| Roy et al. [98] | 50 | 3.8 | 1.32 | 0.3776 | 1 |
| Okuyama et al. [99]. | 100 | 2 | 810 | 0.1178 | 1 |

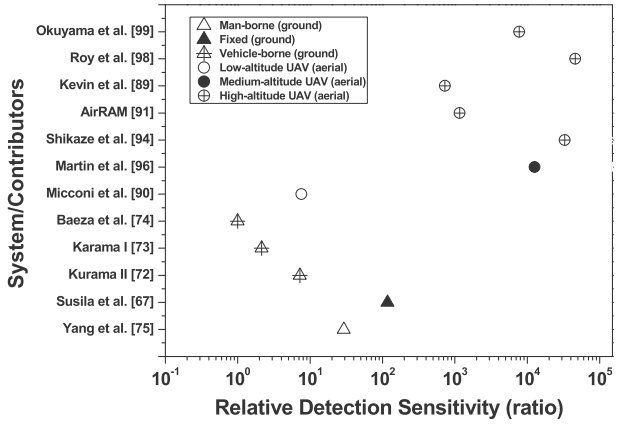


**Fig. 4.** Relative detection sensitivities of various detection platforms capable of performing mapping fallout.

Eq. (3) for the various detector systems capable of performing mapping fallout and scale it appropriately to obtain a plot of relative detection sensitivity (Fig. 4). For illustration, UAVs are considered under three groups. The low-altitude UAVs are restricted to a height of up to 10 m. Medium altitude UAVs can operate between ten and 30 m. High altitude UAVs can navigate beyond 30 m. From Fig. 4, it is evident that vehicle-borne ground detection systems offer the best detection sensitivity. At the other extreme, high-altitude UAVs have the least detection sensitivity, with about four orders of magnitude lower compared to ground vehicle-borne systems. In general, ground-borne systems extend better detection sensitivity than airborne platforms. The existing high-altitude airborne systems provide excellent advantages over ground-based systems in terms of speedy creation of radiation maps. Yet, it is incapable of detecting subtler levels of radiation. From Fig. 4, we can deduce that low-altitude UAV offers detection sensitivity comparable to vehicle-borne systems. Hence, in addition to integration time, energy resolution, and intrinsic efficiency, detector altitude also plays a vital role in influencing detection sensitivity. By optimizing on detector altitude and replacing a single high-altitude UAV, which is generally expensive with a few low-cost medium-altitude or low-altitude UAVs, the advantages offered by high-altitude UAV can be sustained without losing on detection sensitivity.

## 3. Conclusion

The current state of research of a front-end ERM system is highly advanced and sophisticated. The design and the fabrication of tailor-made building blocks, namely, detector active material and an accurately engineered detection platform have contributed significantly to this advancement. The synthesis of novel active materials with improved detection characteristics is a key development for the advancement of the ERM system. Scintillation active materials – $LaCl_3$:Ce, $LaBr_3$:Ce, $CeBr_3$:Ce and $KSr_2I_5$:Eu have been demonstrated to have an incredible energy resolution of less than 3%. Scintillation active materials, hitherto known only for their counting efficiency, now also have an excellent energy resolution ranging from 2 to 3%. The result is that a single detection crystal can be used for both radiation fallout mapping (needs excellent counting efficiency) and spectroscopy processing (needs remarkable energy resolution). Solid-state detector material particularly CZT is clearly winning over its predecessor - HPGe in ERM based detectors, owing to the former's capability of room temperature operation (circumventing the requirement of heavy cooling equipment). Air-borne deployment of ERM systems is attractive and efficient. UAVs are extensively used off late in air-borne ERM. Complementing air-borne deployment is the ground-based detector platform. Ground-based detection methods using smartphones and mobile robots are laudable.

The above-mentioned advancements are commendable, yet there is scope for significant improvements in several areas. There is a dire need for seamlessly combining the operation of the air-borne and ground-based vehicle into a single hybrid autonomous system. Such a system has the potential to overcome the shortcomings of both of the air-borne and the ground-based systems. The present-day ERM use conventional detectors which can be called “proximity detectors” since the radiation interacts directly with these detectors, requiring them to be co-located with the radioactive source. We also have, in contrast, “remote detectors” which work on secondary effects resulting in the interaction of radiation from the radioactive source in its neighborhood. Examples of remote detectors are Lidar, Active Radar, Passive Microwave (21 cm line) Radar and hyperspectral imagers [107] . The “proximity detectors” usually do not allow detection greater than a few hundred meters from the source whereas “remote detectors” can be used to detect radioactive emission at far off distance, typically in the range from few tens of kilometers to few hundreds of kilometers. Nevertheless, “proximity detectors” had been employed in remote monitoring systems such as the Vela satellite radiation monitoring system [108]. However, such satellite-based systems have the limitation of sensing only nuclear explosions with the aid of an optical detector called as “bhang-meter” and cannot be used for ERM because nuclear power plant accidents are seldom accompanied by a nuclear explosion. The use of “remote detectors” besides increasing the field of view when used as an air-borne monitor also have the advantage of being used far away from the place of disaster, and thus both the equipment and operating personnel are shielded from the elevated radiation levels that result at the time of an accident. However, “remote detectors” are still in their infancy and need enhancements in detection calibration techniques to provide a reliable measure of radioactive count rate.

## Declaration of competing interest

The authors declare that they have no known competing financial interests or personal relationships that could have appeared to influence the work reported in this paper.

## Acknowledgment

The authors would like to express their sincere gratitude to Dr. G. Haridas, Health Physics Division, Bhabha Atomic Research Centre

(BARC), Mumbai, INDIA for providing a thorough review and useful suggestions. The authors also like to thank Dr. Kanwal Jeet Singh Sokhey, Thin Film Lab, Synchrotron Utilization Section, Raja Ramanna Center of Advanced Technology(RRCAT), Indore, Madhya Pradesh, INDIA for his constant encouragement and thoughts during the entire course of this manuscript preparation. Finally, the authors also acknowledge the independent review and comments given by Dr. Sharat Chandra, Materials Physics Division, Materials Science Group, Indira Gandhi Centre for Atomic Research (IGCAR) Kalpakkam 603102, TN, INDIA. Of course, these comments enabled us to improve the quality of the manuscript significantly.

## References

[1] F. El Ghissassi, R. Baan, K. Straif, Y. Grosse, B. Secretan, V. Bouvard, L. Benbrahim-Tallaa, N. Guha, C. Freeman, L. Galichet, others, A review of human carcinogens - part D: radiation, Lancet Oncol. 10 (2009) 751–752.
[2] I.A.E. Association, Others, Power Reactor Information System, 2015. Japan (Accessed January 2015).
[3] B.K. Sovacool, A critical evaluation of nuclear power and renewable electricity in Asia, J. Contemp. Asia 40 (2010) 369–400.
[4] D.C.W. Sanderson, J.M. Ferguson, The European capability for environmental airborne gamma ray spectrometry, Radiat. Protect. Dosim. 73 (1997) 213–218.
[5] A. Hasegawa, T. Ohira, M. Maeda, S. Yasumura, K. Tanigawa, Emergency responses and health consequences after the Fukushima accident; evacuation and relocation, Clin. Oncol. 28 (2016) 237–244.
[6] J.W. MacFarlane, O.D. Payton, A.C. Keatley, G.P.T. Scott, H. Pullin, R.A. Crane, M. Smilion, I. Popescu, V. Curlea, T.B. Scott, Lightweight aerial vehicles for monitoring, assessment and mapping of radiation anomalies, J. Environ. Radioact. 136 (2014) 127–130.
[7] M.F. L'Annunziata, Handbook of Radioactivity Analysis, Academic Press, 2012.
[8] G.F. Knoll, Radiation Detection and Measurement, John Wiley & Sons, 2010.
[9] S. Del Sordo, L. Abbene, E. Caroli, A.M. Mancini, A. Zappettini, P. Ubertini, Progress in the development of CdTe and CdZnTe semiconductor radiation detectors for astrophysical and medical applications, Sensors 9 (2009) 3491–3526.
[10] A.S. Novikov, S.E. Ulin, I. V Chernysheva, V. V Dmitrenko, V.M. Grachev, D. V Petrenko, A.E. Shustov, Z.M. Uteshev, K.F. Vlasik, Xenon detector with high energy resolution for gamma-ray line emission registration, in: Hard X-Ray, Gamma-Ray, Neutron Detect. Phys. XVI, 2014, p. 921318.
[11] S.V. Naydenov, V.D. Ryzhikov, Theoretical analysis of physical limits of energy resolution for detectors of scintillator-photodiode type and ways to improve their spectrometric characteristics, in: Hard X-Ray Gamma-Ray Detect. Phys. V, 2004, pp. 261–271.
[12] B.D. Milbrath, A.J. Peurrung, M. Bliss, W.J. Weber, Radiation detector materials: an overview, J. Mater. Res. 23 (2008) 2561–2581.
[13] A.T. Lintereur, W. Qiu, J.C. Nino, J.E. Baciak, Iodine based compound semiconductors for room temperature gamma-ray spectroscopy, Opt. Photonics Glob. Homel. Secur. IV (2008) 694503.
[14] D. Pennicard, B. Pirard, O. Tolbanov, K. Iniewski, Semiconductor materials for x-ray detectors, MRS Bull. 42 (2017) 445–450.
[15] S.J. Bell, P. Aitken-Smith, S. Beeke, S.M. Collins, P.H. Regan, R. Shearman, A comparison of emerging gamma detector technologies for airborne radiation monitoring, J. Phys. Conf. Ser. (2016) 12010.
[16] A.E. Bolotnikov, S. Babalola, G.S. Camarda, Y. Cui, S.U. Egarievwe, R. Hawrami, A. Hossain, G. Yang, R.B. James, Te inclusions in CZT detectors: new method for correcting their adverse effects, IEEE Trans. Nucl. Sci. 57 (2010) 910–919.
[17] A.E. Bolotnikov, N.M. Abdul-Jabbar, S. Babalola, G.S. Camarda, Y. Cui, A. Hossain, E. Jackson, H. Jackson, J.R. James, A.L. Luryi, others, Optimization of virtual Frisch-grid CdZnTe detector designs for imaging and spectroscopy of gamma rays, in: hard X-Ray Gamma-Ray Detect, Phys IX (2007) 670603.
[18] V.L.A. Kosyachenko, T. Aoki, C.P. Lambropoulos, V.A. Gnatyuk, E.V. Grushko, V.M. Sklyarchuk, O.L. Maslyanchuk, O.F. Sklyarchuk, A. Koike, High energy resolution CdTe Schottky diode $\gamma$-ray detectors, Nucl. Sci. Symp. Med. Imaging Conf. (NSS/MIC), 2012 (2012) 4156–4164. IEEE.
[19] V. Gnatyuk, V. Sklyarchuk, T. Aoki, A. Koike, W. Pecharapa, Development of CdTe-based nuclear radiation sensors and related devices, AIP Conf. Proc. (2018) 20012.
[20] H. Haidar, F. Liu, H. Yuan, Calculation of scintillation properties of Ø1 ″$\times$ 1 ″of the lanthanum bromide scintillation detector using MCNP simulation and experiment, J. Phys. Conf. Ser. (2018) 12063.
[21] S.N. Pyae, V.M. Grachev, V.V. Dmitrenko, S.E. Ulin, K.F. Vlasik, Z.M. Uteshev, A.E. Shustov, A.S. Novikov, D.V. Petrenko, I.V. Chernysheva, Xenon gamma-detector applicability for identification and characterization of radioactive waste, Phys. Procedia. 74 (2015) 352–356.
[22] B. Ayaz-Maierhafer, T.A. DeVol, Determination of absolute detection efficiencies for detectors of interest in homeland security, Nucl. Instruments Methods Phys. Res. Sect. A Accel. Spectrometers, Detect. Assoc. Equip. 579 (2007) 410–413.
[23] G.A. Kumar, I. Mazumdar, D.A. Gothe, Experimental measurements and GEANT4 simulations for a comparative study of efficiencies of LaBr3: Ce, NaI (Tl), and BaF2, Nucl. Instruments Methods Phys. Res. Sect. A Accel. Spectrometers, Detect. Assoc. Equip. 610 (2009) 522–529.
[24] C.K. Eun, Y.B. Gianchandani, A wireless-enabled microdischarge-based radiation detector utilizing stacked electrode arrays for enhanced detection efficiency, J. Microelectromechanical Syst. 20 (2011) 636–643.
[25] E.R. Siciliano, J.H. Ely, R.T. Kouzes, B.D. Milbrath, J.E. Schweppe, D.C. Stromswold, Comparison of PVT and NaI (Tl) scintillators for vehicle portal monitor applications, Nucl. Instruments Methods Phys. Res. Sect. A Accel. Spectrometers, Detect. Assoc. Equip. 550 (2005) 647–674.
[26] A. Oberstedt, S. Oberstedt, R. Billnert, W. Geerts, F.-J. Hambsch, J. Karlsson, Identification of prompt fission $\gamma$-rays with lanthanum-chloride scintillation detectors, Nucl. Instruments Methods Phys. Res. Sect. A Accel. Spectrometers, Detect. Assoc. Equip. 668 (2012) 14–20.
[27] A. Oberstedt, R. Billnert, S. Oberstedt, Neutron measurements with lanthanum–bromide scintillation detectors: a first approach, Nucl. Instruments Methods Phys. Res. Sect. A Accel. Spectrometers, Detect. Assoc. Equip. 708 (2013) 7–14.
[28] A. Zoglauer, M. Galloway, M. Amman, S.E. Boggs, J.S. Lee, P.N. Luke, L. Mihailescu, K. Vetter, C.B. Wunderer, First results of the high efficiency multi-mode imager (HEMI), in: Nucl. Sci. Symp. Conf. Rec. (NSS/MIC), 2009, IEEE, 2009, pp. 887–891.
[29] P.N. Luke, M. Amman, J.S. Lee, C.Q. Vu, Pocket-size CdZnTe gamma-ray spectrometer, IEEE Trans. Nucl. Sci. 52 (2005) 2041–2044.
[30] M. Yousaf, T. Akyurek, S. Usman, A comparison of traditional and hybrid radiation detector dead-time models and detector behavior, Prog. Nucl. Energy 83 (2015) 177–185.
[31] S. Usman, A. Patil, Radiation detector deadtime and pile up: a review of the status of science, Nucl. Eng. Technol. 50 (7) (2018) 1006–1016.
[32] R. Malhotra, Y.B. Gianchandani, A microdischarge-based neutron radiation detector utilizing a stacked arrangement of micromachined steel electrodes with gadolinium film for neutron conversion, IEEE Sensor. J. 15 (2015) 3863–3870.
[33] A. Migdall, S.V. Polyakov, J. Fan, J.C. Bienfang, Single-photon Generation and Detection: Physics and Applications, Academic Press, 2013.
[34] N. Tsoulfanidis, Measurement and Detection of Radiation, CRC press, 2010.
[35] V.E. Kutny, A.V. Rybka, L.N. Davydov, A.O. Pudov, S.A. Sokolov, G.A. Kholomeyev, S.I. Melnikov, A.A. Turchin, Gamma-ray detector based on high pressure xenon for radiation and environmental safety, Probl. At. Sci. Technol. (2017) 103–108.
[36] F.G.A. Quarati, M.S. Alekhin, K.W. Krämer, P. Dorenbos, Co-doping of CeBr3 scintillator detectors for energy resolution enhancement, Nucl. Instruments Methods Phys. Res. Sect. A Accel. Spectrometers, Detect. Assoc. Equip. 735 (2014) 655–658.
[37] M.S. Alekhin, D.A. Biner, K.W. Krämer, P. Dorenbos, Optical and scintillation properties of CsBa2I5: Eu2+, J. Lumin. 145 (2014) 723–728.
[38] Z.T. Kang, R. Rosson, B. Barta, C. Han, J.H. Nadler, M. Dorn, B. Wagner, B. Kahn, GdBr3: Ce in glass matrix as nuclear spectroscopy detector, Radiat. Meas. 48 (2013) 7–11.
[39] A.O. Pudov, A.S. Abyzov, S.A. Sokolov, L.N. Davydov, A.V. Rybka, V.E. Kutny, S.I. Melnikov, G.A. Kholomyeyev, S.A. Leonov, A.A. Turchin, Measurements and modeling of charge carrier lifetime in compressed xenon, Nucl. Instruments Methods Phys. Res. Sect. A Accel. Spectrometers, Detect. Assoc. Equip. 892 (2018) 98–105.
[40] W. Chewpraditkul, K. Sreebunpeng, M. Nikl, J.A. Mares, K. Nejezchleb, A. Phunpueok, C. Wanarak, Comparison of Lu3Al5O12: Pr3+ and Bi4Ge3O12 scintillators for gamma-ray detection, Radiat. Meas. 47 (2012) 1–5.
[41] M. Grodzicka, M. Moszyński, T. Szcz\keśniak, M. Kapusta, M. Szawłowski, D. Wolski, Energy resolution of small scintillation detectors with SiPM light readout, J. Instrum. 8 (2013), P02017.
[42] T. Huang, Q. Fu, S. Lin, B. Wang, NaI (Tl) scintillator read out with SiPM array for gamma spectrometer, Nucl. Instruments Methods Phys. Res. Sect. A Accel. Spectrometers, Detect. Assoc. Equip. 851 (2017) 118–124.
[43] T.J. Hajagos, C. Liu, N.J. Cherepy, Q. Pei, High-Z sensitized plastic scintillators: a review, Adv. Mater. (2018) 1706956.
[44] P. Wangyang, C. Gong, G. Rao, K. Hu, X. Wang, C. Yan, L. Dai, C. Wu, J. Xiong, Recent advances in halide perovskite photodetectors based on different dimensional materials, Adv. Opt. Mater. 6 (2018), 1701302.
[45] O. Nazarenko, S. Yakunin, V. Morad, I. Cherniukh, M. V Kovalenko, Single crystals of caesium formamidinium lead halide perovskites: solution growth and gamma dosimetry, NPG Asia Mater. 9 (2017) e373.
[46] T. Koike, S. Uno, T. Uchida, M. Sekimoto, T. Murakami, K. Miyama, M. Shoji, T. Fujiwara, E. Nakano, J. Chiba, A new gamma-ray detector with gold-plated gas electron multiplier, Nucl. Instruments Methods Phys. Res. Sect. A Accel. Spectrometers, Detect. Assoc. Equip. 648 (2011) 180–185.
[47] G. Takoudis, S. Xanthos, A. Clouvas, M. Antonopoulos-Domis, C. Potiriadis, J. Silva, Spatial and spectral gamma-ray response of plastic scintillators used in portal radiation detectors; comparison of measurements and simulations, Nucl. Instruments Methods Phys. Res. Sect. A Accel. Spectrometers, Detect. Assoc. Equip. 599 (2009) 74–81.
[48] S. Das, J. Saini, A.K. Dubey, Measurement of decay time constant of a plastic scintillator by a delayed coincidence method, DAE Symp. Nucl. Phys. (2015) 1068–1069.

[49] M. Nikl, A. Yoshikawa, Recent R&D trends in inorganic single-crystal scintillator materials for radiation detection, Adv. Opt. Mater. 3 (2015) 463–481.
[50] L. Stand, M. Zhuravleva, B. Chakoumakos, J. Johnson, A. Lindsey, C.L. Melcher, Scintillation properties of Eu 2+-doped KBa 2 I 5 and K 2 Bai 4, J. Lumin. 169 (2016) 301–307.
[51] L. Stand, M. Zhuravleva, A. Lindsey, C.L. Melcher, Growth and characterization of potassium strontium iodide: a new high light yield scintillator with 2.4% energy resolution, Nucl. Instruments Methods Phys. Res. Sect. A Accel. Spectrometers, Detect. Assoc. Equip. 780 (2015) 40–44.
[52] E.D. Bourret-Courchesne, G. Bizarri, R. Borade, Z. Yan, S.M. Hanrahan, G. Gundiah, A. Chaudhry, A. Canning, S.E. Derenzo, Eu2+-doped Ba2CsI5, a new high-performance scintillator, Nucl. Instruments Methods Phys. Res. Sect. A Accel. Spectrometers, Detect. Assoc. Equip. 612 (2009) 138–142.
[53] M.S. Alekhin, S. Weber, K.W. Krämer, P. Dorenbos, Optical properties and defect structure of Sr2+ co-doped LaBr3: 5% Ce scintillation crystals, J. Lumin. 145 (2014) 518–524.
[54] K.H. Kim, A.E. Bolotnikov, G.S. Camarda, R. Tappero, A. Hossain, Y. Cui, J. Franc, L. Marchini, A. Zappettini, P. Fochuk, others, New approaches for making large-volume and uniform CdZnTe and CdMnTe detectors, IEEE Trans. Nucl. Sci. 59 (2012) 1510–1515.
[55] C. Leak, W. Koehler, S. O'Neal, Z. He, K. Hitomi, Recent results from pixelated TlBr detectors with Tl electrodes operated at room-temperature, in: Nucl. Sci. Symp. Med. Imaging Conf. Room-Temperature Semicond. Detect. Work. (NSS/MIC/RTSD), 2016, 2016, pp. 1–3.
[56] M. Streicher, Y. Zhu, F. Zhang, Y.A. Boucher, C.G. Wahl, H. Yang, Z. He, A portable 2$\times$ 2 digital 3D CZT imaging spectrometer system, in: Nucl. Sci. Symp. Med. Imaging Conf. (NSS/MIC), 2014, IEEE, 2014, pp. 1–3.
[57] S. Watanabe, T. Takahashi, Y. Okada, C. Sato, M. Kouda, T. Mitani, Y. Kobavashi, K. Nakazawa, Y. Kuroda, M. Onishi, CdTe stacked detectors for Gamma-ray detection, in: Nucl. Sci. Symp. Conf. Rec. 2001, IEEE, 2001, pp. 2434–2438.
[58] J. Saegusa, K. Kawasaki, A. Mihara, M. Ito, M. Yoshida, Determination of detection efficiency curves of HPGe detectors on radioactivity measurement of volume samples, Appl. Radiat. Isot. 61 (2004) 1383–1390.
[59] Y. He, L. Matei, H.J. Jung, K.M. McCall, M. Chen, C.C. Stoumpos, Z. Liu, J.A. Peters, D.Y. Chung, B.W. Wessels, others, High spectral resolution of gamma-rays at room temperature by perovskite CsPbBr 3 single crystals, Nat. Commun. 9 (2018) 1609.
[60] M. Isaksson, C.L. Raaf, Environmental Radioactivity and Emergency Preparedness, CRC Press, 2017.
[61] F.G.A. Quarati, P. Dorenbos, J. der Biezen, A. Owens, M. Selle, L. Parthier, P. Schotanus, Scintillation and detection characteristics of high-sensitivity CeBr3 gamma-ray spectrometers, Nucl. Instruments Methods Phys. Res. Sect. A Accel. Spectrometers, Detect. Assoc. Equip. 729 (2013) 596–604.
[62] H. Toivonen, Airborne gamma spectrometry—towards integration of European operational capability, Radiat. Protect. Dosim. 109 (2004) 137–140.
[63] D. Connor, P.G. Martin, T.B. Scott, Airborne radiation mapping: overview and application of current and future aerial systems, Int. J. Rem. Sens. 37 (2016) 5953–5987.
[64] K. Saito, Mapping and modelling of radionuclide distribution on the ground due to the Fukushima accident, Radiat. Protect. Dosim. 160 (2014).
[65] A.-J. Garcia-Sanchez, E.A. Garcia Angosto, P.A. Moreno Riquelme, A. Serna Berna, D. Ramos-Amores, Ionizing radiation measurement solution in a hospital environment, Sensors 18 (2018) 510.
[66] M.I. Kaniu, H.K. Angeyo, I.G. Darby, L.M. Muia, Rapid in-situ radiometric assessment of the Mrima-Kiruku high background radiation anomaly complex of Kenya, J. Environ. Radioact. 188 (2018) 47–57.
[67] I.P. Susila, A. Yuniarto, C. Cahyana, Monitoring and analysis of environmental gamma dose rate around serpong nuclear complex, At. Indones. 43 (2017) 87–92.
[68] Y. Omori, H. Wakamatsu, A. Sorimachi, T. Ishikawa, Radiation survey on Fukushima Medical University premises about four years after the Fukushima nuclear disaster, Fukushima J. Med. Sci. 62 (2016) 1–17.
[69] R.M. Vázquez, E. Gutiérrez, Mobile robot for gamma radiation detection with long range remote control, Mechatronics, Electron. Automot. Eng. (ICMEAE), 2015 Int. Conf. (2015) 175–180.
[70] S. Kobayashi, T. Shinomiya, H. Kitamura, T. Ishikawa, H. Imaseki, M. Oikawa, S. Kodaira, N. Miyaushiro, Y. Takashima, Y. Uchihori, Radioactive contamination mapping of northeastern and eastern Japan by a car-borne survey system, Radi-Probe, J. Environ. Radioact. 139 (2015) 281–293.
[71] S. Syarbaini, B. Bunawas, I.P. Susila, Design and development of carborne survey equipment, At. Indones. 41 (2015) 97–102.
[72] M. Andoh, Y. Nakahara, S. Tsuda, T. Yoshida, N. Matsuda, F. Takahashi, S. Mikami, N. Kinouchi, T. Sato, M. Tanigaki, others, Measurement of air dose rates over a wide area around the Fukushima Dai-ichi Nuclear Power Plant through a series of car-borne surveys, J. Environ. Radioact. 139 (2015) 266–280.
[73] M. Tanigaki, R. Okumura, K. Takamiya, N. Sato, H. Yoshino, H. Yamana, Development of a car-borne γ-ray survey system, KURAMA, Nucl. Instruments Methods Phys. Res. Sect. A Accel. Spectrometers, Detect. Assoc. Equip. 726 (2013) 162–168.
[74] A. Baeza, J.A. Corbacho, J. Miranda, Design and implementation of a mobile radiological emergency unit integrated in a radiation monitoring network, IEEE Trans. Nucl. Sci. 60 (2013) 1400–1407.
[75] Y. Ishigaki, Y. Matsumoto, R. Ichimiya, K. Tanaka, Development of mobile radiation monitoring system utilizing smartphone and its field tests in Fukushima, IEEE Sensor. J. 13 (2013) 3520–3526.
[76] D. Williams, H. Bisby, The aerial survey of terrestrial radioactivity, Proc. IEE-Part B Electron. Commun. Eng. 108 (1961) 403–412.
[77] C. Nuccetelli, D.M. Castelluccio, E. Cisbani, S. Frullani, Experience at the istituto superiore di sanità on environmental research and monitoring with in-situ techniques, Situ Anal. Charact. Contam. Sites Using Nucl. Spectrom. Tech. (n.d.) 119.
[78] R.C. Runkle, L.E. Smith, A.J. Peurrung, The photon haystack and emerging radiation detection technology, J. Appl. Phys. 106 (2009) 7.
[79] S.D. Billings, B.R. Minty, G.N. Newsam, Deconvolution and spatial resolution of airborne gamma-ray surveys, Geophysics 68 (2003) 1257–1266.
[80] D.M. Pfund, K.D. Jarman, B.D. Milbrath, S.D. Kiff, D.E. Sidor, Low count anomaly detection at large standoff distances, IEEE Trans. Nucl. Sci. 57 (2010) 309–316.
[81] M. Weinstein, A. Heifetz, R. Klann, Detection of nuclear sources in search survey using dynamic quantum clustering of gamma-ray spectral data, Eur. Phys. J. Plus. 129 (2014) 239.
[82] J.E. McLaughlin, H.L. Beck, Environmental radiation dosimetry for nuclear facilities and problems, IEEE Trans. Nucl. Sci. 20 (1973) 36–42.
[83] A.G. Darnley, The Relevance of Airborne and Ground Gamma Ray Spectrometry to Global Geochemical Baselines, Appl. Uranium Explor. Data Tech. Environ. Stud. IAEA-TECDOC-827, IAEA, Vienna, 1995, pp. 47–58.
[84] D.C.W. Sanderson, J.D. Allyson, A.N. Tyler, E.M. Scott, Environmental Applications of Airborne Gamma Spectrometry, 1995.
[85] I. Winkelmann, C. Strobl, M. Thomas, Aerial measurements of artificial radionuclides in Germany in case of a nuclear accident, J. Environ. Radioact. 72 (2004) 225–231.
[86] Z.G. Burson, Airborne surveys of terrestrial gamma radiation in environmental research, IEEE Trans. Nucl. Sci. 21 (1974) 558–571.
[87] S. Okuyama, T. Torii, Y. Nawa, I. Kinoshita, A. Suzuki, M. Shibuya, N. Miyazaki, Development of a remote radiation monitoring system using unmanned helicopter, Int. Congr. Ser. (2005) 422–423.
[88] J. Towler, B. Krawiec, K. Kochersberger, Radiation mapping in post-disaster environments using an autonomous helicopter, Rem. Sens. 4 (2012) 1995–2015.
[89] K. Kochersberger, K. Kroeger, B. Krawiec, E. Brewer, T. Weber, Post-disaster remote sensing and sampling via an autonomous helicopter, J. Field Robot. 31 (2014) 510–521.
[90] G. Micconi, J. Aleotti, S. Caselli, G. Benassi, N. Zambelli, A. Zappettini, Haptic guided UAV for detection of radiation sources in outdoor environments, Res. Educ. Dev. Unmanned Aer. Syst. (RED-UAS), 2015 Work. (2015) 265–271.
[91] S. Dadon, A. Broide, M. Sheinfeld, Y. Kadmon, Y. Cohen, I. Halevy, Radioactive contamination estimation by airborne survey based NaI detectors, IEEE Trans. Nucl. Sci. 63 (2016) 630–633.
[92] Y. Sato, S. Ozawa, Y. Terasaka, M. Kaburagi, Y. Tanifuji, K. Kawabata, H.N. Miyamura, R. Izumi, T. Suzuki, T. Torii, Remote radiation imaging system using a compact gamma-ray imager mounted on a multicopter drone, J. Nucl. Sci. Technol. 55 (2018) 90–96.
[93] S. Mochizuki, J. Kataoka, L. Tagawa, Y. Iwamoto, H. Okochi, N. Katsumi, S. Kinno, M. Arimoto, T. Maruhashi, K. Fujieda, others, First demonstration of aerial gamma-ray imaging using drone for prompt radiation survey in Fukushima, J. Instrum. 12 (2017) P11014.
[94] Y. Shikaze, Y. Nishizawa, Y. Sanada, T. Torii, J. Jiang, K. Shimazoe, H. Takahashi, M. Yoshino, S. Ito, T. Endo, others, Field test around Fukushima Daiichi nuclear power plant site using improved Ce: Gd3 (Al, Ga) 5O12 scintillator Compton camera mounted on an unmanned helicopter, J. Nucl. Sci. Technol. 53 (2016) 1907–1918.
[95] Y. Sanada, T. Torii, Aerial radiation monitoring around the Fukushima Dai-ichi nuclear power plant using an unmanned helicopter, J. Environ. Radioact. 139 (2015) 294–299.
[96] P.G. Martin, O.D. Payton, J.S. Fardoulis, D.A. Richards, T.B. Scott, The use of unmanned aerial systems for the mapping of legacy uranium mines, J. Environ. Radioact. 143 (2015) 135–140.
[97] K. Boudergui, F. Carrel, T. Domenech, N. Guenard, J.-P. Poli, A. Ravet, V. Schoepff, R. Woo, Development of a drone equipped with optimized sensors for nuclear and radiological risk characterization, Adv. Nucl. Instrum. Meas. Methods Their Appl. (ANIMMA), 2011 2nd Int. Conf. (2011) 1–9.
[98] R. Pöllänen, H. Toivonen, K. Peräjärvi, T. Karhunen, T. Ilander, J. Lehtinen, K. Rintala, T. Katajainen, J. Niemelä, M. Juusela, Radiation surveillance using an unmanned aerial vehicle, Appl. Radiat. Isot. 67 (2009) 340–344.
[99] S. Okuyama, T. Torii, A. Suzuki, M. Shibuya, N. Miyazaki, A remote radiation monitoring system using an autonomous unmanned helicopter for nuclear emergencies, J. Nucl. Sci. Technol. 45 (2008) 414–416.
[100] R.L. Grasty, B.R.S. Minty, A Guide to the Techncial Specifications for Airborne Gamma-Ray Surveys, Citeseer, 1990.
[101] M. Alamaniotis, J. Mattingly, L.H. Tsoukalas, Kernel-based machine learning for background estimation of NaI low-count gamma-ray spectra, IEEE Trans. Nucl. Sci. 60 (2013) 2209–2221.
[102] T. Smith, S. Cao, K.J. Kearfott, Temporal fluctuations in indoor background gamma radiation using NaI (Tl), Health Phys. 114 (2018) 360–372.
[103] K. Kumagai, H. Ookubo, H. Kimura, Discrimination between natural and other gamma ray sources from environmental gamma ray dose rate monitoring data, Radiat. Protect. Dosim. 167 (2015) 293–297.
[104] K.A.P. Kumar, G.A.S. Sundaram, R. Thiruvengadathan, Advances in detection

algorithms for radiation monitoring, J. Environ. Radioact. 217 (2020), 106216.
[105] E.Z. Sombrito, M.C. Tangonan, A.D. Bulos, Detector Efficiency and Energy Calibration of the CRD HPGe Gamma Spectrometer System, 1989.
[106] J. Rajendran, G.A.S. Sundaram, Design and evaluation of printed log periodic dipole antenna for an L band electrically steerable array system, Comput. Syst. Commun. (ICCSC), 2014 First Int. Conf. (2014) 311–316.
[107] M. Kort, Weapons of Mass Destruction, Infobase Publishing, 2010.
[108] M.J Berger, J.H. Hubbell, S.M. Seltzer, J. Chang, J.S. Coursey, R. Sukumar, D.S. Zucker, K. Olsen, XCOM: photon cross section database, National Institute of Standards and Technology, Gaithersburg, Gaithersburg, MD. (2005). http://physics. nist. gov/xcom.